Journal of Molecular Spectroscopy 253 (2009) 99–105

Contents lists available at ScienceDirect

Journal of Molecular Spectroscopy

journal homepage: www.elsevier.com/locate/jms

Sub-millimeter wave spectroscopy of the C_3H radical: Ro-vibrational transitions from ground to the lowest bending state

M. Caris [a], T.F. Giesen [a,*], C. Duan [a,1], H.S.P. Müller [a], S. Schlemmer [a], K.M.T. Yamada [b,2]

[a] I. Physikalisches Institut, Universität zu Köln, Zülpicher Str. 77, 50937 Cologne, Germany
[b] AIST, Tsukuba-west, Onogawa 16-1, Tsukuba, Ibaraki 305-8569, Japan

ARTICLE INFO

Article history:
Received 22 September 2008
Available online 6 November 2008

Keywords:
C_3H
Low bending mode
Renner–Teller effect
Terahertz spectroscopy

ABSTRACT

Linear C_3H in its ($X^2\Pi$) electronic ground state possesses strong Renner–Teller coupling in the two lowest bending modes, v_4 and v_5. The $^2\Sigma^\mu$ level of the $v_4 = 1$ bending mode is shifted towards lower energies and is supposed to lie only 20.3 cm^{-1} above the ground state [S. Yamamoto, S. Saito, H. Suzuki, S. Deguchi, N. Kaifu, S. Ishikawa, M. Ohishi, Astrophys. J. 348 (1990) 363]. In the present study, first measurements of ro-vibrational transitions from the $^2\Pi_{3/2}$ ground state to the $^2\Sigma^\mu$ lowest vibrational state were performed using a Terahertz spectrometer equipped with a supersonic jet nozzle. Rotational levels of the $^2\Pi_{3/2}$ and $v_4 = 1(^2\Sigma^\mu)$ state are close in energy and a crossing of the rotational energy ladders occurs between $J = 24.5$ and 25.5. A strong vibronic coupling leads to a significant intensity enhancement of $^2\Pi_{3/2} - {}^2\Sigma^\mu$ ro-vibrational transitions. The search for ro-vibrational transitions was facilitated by measurements on pure rotational transitions in the $^2\Pi_{1/2}$, $^2\Pi_{3/2}$ and $v_4 = 1(^2\Sigma^\mu)$ states, substantially extending the former data set published by Yamamoto et al. Data analysis yields an accurate value for the $v_4 = 1(^2\Sigma^\mu)$ energy level which has been found to lie 609.9771(42) GHz or 20.34664(14) cm^{-1} above the $^2\Pi$ ground state. Furthermore, the value of the vibronic coupling constant β has been improved significantly and determined as 1231.77(51) MHz. The new set of spectroscopic parameters obtained in the present study permits very reliable frequency predictions into the Terahertz region.

1. Introduction

Carbon chain molecules play an important role in astrochemical processes of cold interstellar clouds and shells of late type carbon stars [1,2]. One of these species is linear C_3H, of which spectral features have been found by Johansson et al. in 1984 in a line survey of the carbon star IRC+10216 [3]. Shortly thereafter, this tentative detection was confirmed by Thaddeus [4] based on extended astrophysical data and first laboratory measurements recorded by Gottlieb et al. [5]. C_3H has two isomeric forms, besides the linear form a cyclic isomer exists which is according to *ab initio* calculations energetically more stable than the linear one. First laboratory spectra and the interstellar detection of cyclic C_3H were published by Yamamoto et al. in 1987, who found several lines in the spectrum of the dark cloud TMC-1 [6].

Linear C_3H has a $^2\Pi$ electronic ground state and its two bending vibrational modes, v_4 and v_5, are perturbed by the Renner–Teller (RT) effect. Pure rotational lines measured in the $v_4(^2\Sigma^\mu)$ vibrationally excited state of linear C_3H and C_3D by Yamamoto et al. [7] show strong vibronic interaction with the $^2\Pi_{3/2}$-component of the ground state. The authors concluded that due to the strong RT coupling the $^2\Sigma^\mu$ state is shifted towards lower energies and lies only 20.3 cm^{-1} above the zero-level of the two $^2\Pi$-components. The molecular structure of linear C_3H was derived from rotational spectra including ^{13}C isotopic species published by Kanada et al. [8]. The same authors reported on the hyperfine structure constants of ^{13}C substituted species which were more accurately determined by McCarthy and Thaddeus [9] using Fourier transform microwave spectroscopy.

Besides the investigations on pure rotational transitions, gas phase spectra of C_3H are rather sparse. Electronic spectra were measured by Ding et al. [10] and recent measurements to characterize cyclic and linear C_3H and C_3H^- via photoelectron spectroscopy were reported by Sheehan et al. [11]. To our knowledge there are no rotationally resolved vibrational spectra of C_3H available. However Jiang et al. measured infrared vibrational band centers of linear and cyclic C_3H trapped in a cold argon matrix [12].

In the present paper, we report on first high resolution gas phase spectra of the v_4 lowest bending mode of linear C_3H. Eight transitions of the $^2\Sigma^\mu - {}^2\Pi_{3/2}$ band system have been measured. For those cases where the interacting energy levels are in

* Corresponding author.
E-mail address: giesen@ph1.uni-koeln.de (T.F. Giesen).
[1] Present address: College of Physical Science and Technology, HuaZhong Normal University, Wuhan 430079, PR China.
[2] Permanent address: A&A Laboratories, Sengataki-Nakaku 523-1, Karuizawa, Nagano 389-0111, Japan.

0022-2852/$ - see front matter © 2008 Elsevier Inc. All rights reserved.
doi:10.1016/j.jms.2008.10.006

resonance, line intensities are enhanced by the vibronic interaction. In addition, 44 pure rotational lines of the three bands $^2\Pi_{1/2}$, $^2\Pi_{3/2}$, and $^2\Sigma^{\mu}$ up to 539 GHz have been recorded to improve molecular parameters.

2. The bending excited state and the Renner–Teller effect

The Renner–Teller (RT) effect in bending states of C_3H has mainly been studied theoretically (see e.g., Perić et al. [13]) besides the experimental work of Yamamoto et al. [7]. The linear four-atomic C_3H radical has two vibrational bending modes, v_4 and v_5, the vibrational angular momenta of which couple with the electronic orbital angular momentum of the $^2\Pi$ state. As a result, each bending vibrational state splits into four components, denoted as $^2\Sigma^{\mu}$, $^2\Sigma^{\kappa}$, $^2\Delta_{3/2}$, and $^2\Delta_{5/2}$. In the absence of the RT and spin–orbit coupling effect these levels are degenerate in energy and should appear near 600 cm^{-1} in case of the v_4 CCH bending mode, and near 300 cm^{-1} in case of the v_5 CCC bending mode. The RT effect lifts the degeneracy of vibronic levels and the $^2\Sigma^{\kappa}$ and $^2\Sigma^{\mu}$ sub-levels are split significantly, as can be seen from Fig. 1. The magnitude of the energy shifts are expressed as $\epsilon_t\,\omega_t$, where ϵ_t and ω_t are the RT parameter and the harmonic frequency of the bending vibration, respectively.

High level *ab initio* calculations by Peric et al. [13] predict the RT coupling to be strongest for the v_4 mode ($\epsilon_4 = -0.8537$) and the energetically lower component (Σ^{μ}) is shifted towards the $^2\Pi$ ground state, whereas the upper component ($^2\Sigma^{\kappa}$) is shifted up to about 1200 cm^{-1}. On the other hand, the RT splitting in the v_5 mode is less pronounced, and the RT parameter is predicted as $\epsilon_5 = 0.3393$. Thus, the origin of the lowest excited $^2\Sigma$ vibronic state can be identified as the $v_4 = 1$ state. This conclusion agrees with that deduced experimentally by Yamamoto et al. [7] from the change in the vibrational energy upon deuterium substitution.

The energy levels are also affected by spin–orbit (SO) coupling. In the present case, however, the SO effect is negligibly small in comparison to the RT splitting. Thus, the two Σ states exhibit a clear Hund's case (b) coupling scheme [14,15]. In such a case the two Σ states can be distinguished as $\Sigma^{\pm}$. Since the RT parameter ϵ_4 is predicted to be negative, we assume in the present study that the $^2\Sigma^{\mu}$ state is $^2\Sigma^{+}$ following Hougen [15]. This assumption had been applied also by Yamamoto et al. [7], but implicitly.

3. Experimental procedure

The Cologne Supersonic Jet Spectrometer for Terahertz Applications, SuJeSTA, was used to record absorption spectra of linear C_3H from 376 to 572 GHz. The molecules were produced in a pulsed electrical discharge-nozzle [16] from an adiabatically expanding gas mixture of C_2H_2 (1.5–2.3%) and CO (40–60%) diluted in He at 1–6 bar backing pressure. The gas mixture was pre-expanding through a pulsed valve with 1 mm orifice into a slit of 3 cm length and 1 mm width. A pair of metal plate electrodes separated (~1 mm) by ceramic spacers is mounted in front of the valve (see Ref. [16] for details). Typically, 800–1100 V discharge voltage were applied to the electrodes and discharge currents of 400–900 mA were measured, depending on gas mixing ratio, backing pressure, and pulse duration. The pulse repetition rate was set to 50 Hz and synchronized to the AC-line frequency. The pulse length of the gas flow was approximately 200 μs followed by a 300 μs discharge pulse. A two stage roots-blower pumping-system of

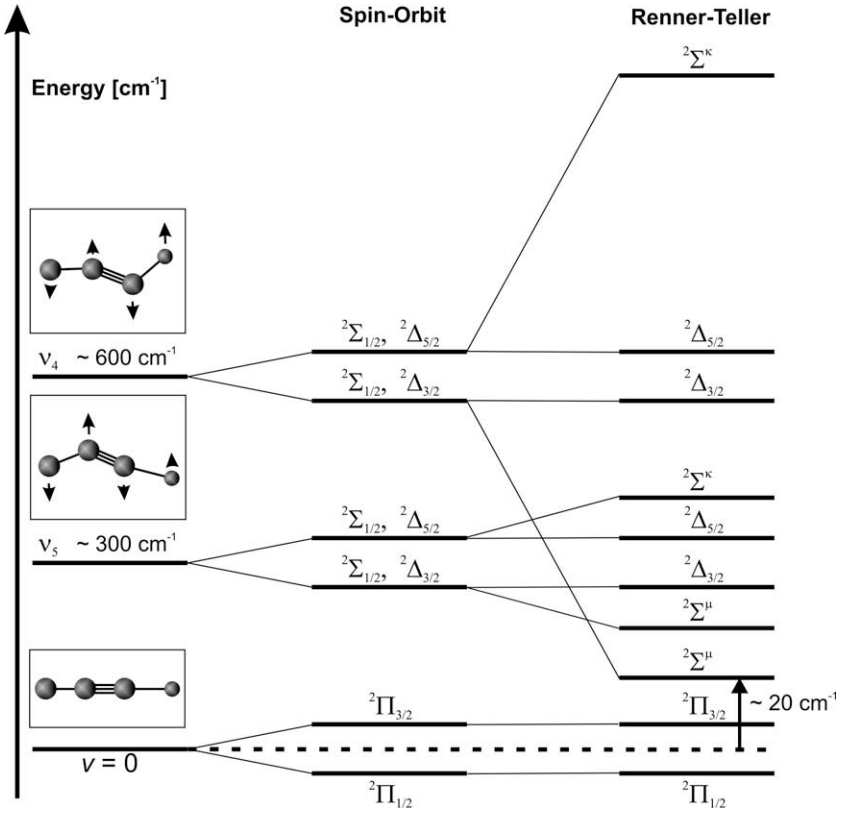

Fig. 1. Energy level diagram of C_3H. The ground state is a regular $^2\Pi$ state, with $^2\Pi_{1/2}$ and $^2\Pi_{3/2}$ states separated by $A_{SO} = 14.4$ cm^{-1} due to spin–orbit coupling. The energy term with $A_{SO} = 0$ cm^{-1} is defined as zero-level (dotted line). The energy levels of the excited bending states, i.e. $v_4 = 1$ and $v_5 = 1$ state, both are split into four substates due to spin–orbit and Renner–Teller interaction: two $^2\Sigma$-components and two $^2\Delta$-component. Due to a strong Renner–Teller effect the $v_4(^2\Sigma^{\mu})$-component is shifted towards lower energies, ~20 cm^{-1} above the zero-level of the ground state.

4600 m^3/h pumping speed provided stable pressure conditions of below 5×10^{-2} mbar inside the vacuum chamber and supersonic expansion of the gas led to adiabatic cooling of rotational transitions down to a few 10 K.

The spectrometer is shown in Fig. 2. Backward wave oscillators (BWOs) were used as radiation sources and a frequency stability of better than 1 kHz was achieved by phase locking the BWO frequency to a rubidium time standard. The sub-millimeter wave radiation intersects the supersonic jet ~5 cm downstream in a perpendicular configuration and a multi-pass optics with six paths is used to further enhance the signal-to-noise ratio. The absorption signal is detected by a low-noise liquid-He cooled InSb hot electron bolometer of high sensitivity. The frequency of the BWO was modulated at 30–45 kHz and phase sensitive detection of the signal was achieved by a lock-in amplifier in 2*f*-mode operation. In addition to the frequency modulation of the radiation source, an on–off modulation of the jet was used for background subtraction through a pair of boxcar integrators. The data acquisition was taken within a 100 μs time window at the end of the discharge pulse which was found to deliver best results for C_3H. The integration time for background subtraction was about 400–500 μs long. The combination of frequency and source modulation (double modulation technique) substantially improved the signal-to-noise ratio and at the same time suppressed standing wave etalon effects.

4. Observed spectra

The frequency range from 376 to 572 GHz has been covered in the present measurements. Pure rotational transitions in the $v = 0(^2\Pi_{1/2})$ and $(^2\Pi_{3/2})$ ground state and $v_4 = 1(^2\Sigma^\mu)$ vibrational excited state have been detected straightforwardly based on results from Yamamoto et al. [7]. Because of vibronic interaction between the $\Pi_{3/2}$ and the $^2\Sigma^\mu$ state, some fine structure components had been predicted with larger uncertainties and were usually observed less closely to the predictions than the remaining lines. Including such transitions in the fit we have reduced the uncertainties both in the energy difference between these states as well as in the coefficient of the vibronic term, β. Eventually, their uncertainties were small enough to locate ro-vibrational transitions with confidence. In total, 14 lines within the $\Pi_{1/2}$ state, 17 lines within the $\Pi_{3/2}$ state, and 13 in the excited $^2\Sigma^\mu$ state have been recorded.

Furthermore, eight ro-vibrational transitions from the ground state to the excited bending state, $v_4 = 1 \leftarrow 0(^2\Sigma^\mu \leftarrow {}^2\Pi_{3/2})$, were measured with high precision. These are the first ro-vibrational transitions of C_3H at all and allow for a precise determination of the $v_4(^2\Pi_{3/2} - {}^2\Sigma^\mu)$ band center. Fig. 3 shows four of the measured lines, three pure rotational transitions of the $\Pi_{1/2}$, $\Pi_{3/2}$, and Σ^μ states and one of the $\Sigma^\mu - \Pi_{3/2}$ ro-vibrational transitions. All measured lines are listed in Tables 1–4 together with the estimated experimental uncertainties. Hyperfine splitting due to the proton's nuclear spin has been resolved for 10 rotational or ro-vibrational transitions, in particular for the transitions near the energy level crossing of the $^2\Sigma^\mu$ and $^2\Pi_{3/2}$ states. Hyperfine splitting for high J levels are usually not resolved but for levels near the crossing point the splitting becomes visible due to the vibronic interaction of ground state and v_4 excited $^2\Sigma^\mu$ state levels, as can be seen from Tables 2–4. Fig. 4 shows the energy level diagram of the two $^2\Pi$ states and the $^2\Sigma^\mu$ state in the region of the energy level crossing.

Disregarding hyperfine interaction, the perturbed wavefunctions for a given state $\psi(J, \Gamma, \gamma)$ can be expressed as linear combination of unperturbed wavefunctions $\psi^0(J, \Gamma', \gamma)$:

$$\psi(J, \Gamma, \gamma) = \sum_{\Gamma'} c_{\Gamma\Gamma'} \psi^0(J, \Gamma', \gamma), \tag{1}$$

where Γ and Γ' indicate the vibronic states $^2\Pi_{1/2}$, $^2\Pi_{3/2}$, and $^2\Sigma^\mu$. The index γ represents the parity of the state. Note that the states with same J and same parity are mixed. The largest perturbations occur at energies of approximately 261.5 cm^{-1} above the zero-level of the ground state, with the maximum value of the square of the diagonal mixing coefficient $c^2 = c^2_{\Gamma\Gamma} = 0.6$. Due to the mixing of wavefunctions the perturbed ro-vibrational transitions borrow intensity from the pure rotational transitions. The intensities of the $J = 25.5 - 24.5$ transitions listed in Table 4 (the last three lines) were indeed observed to be about 2–5 times stronger than the other ro-vibrational transitions listed in the same table. In Fig. 5 the effect of the resonance on the energy levels is shown on an expanded scale.

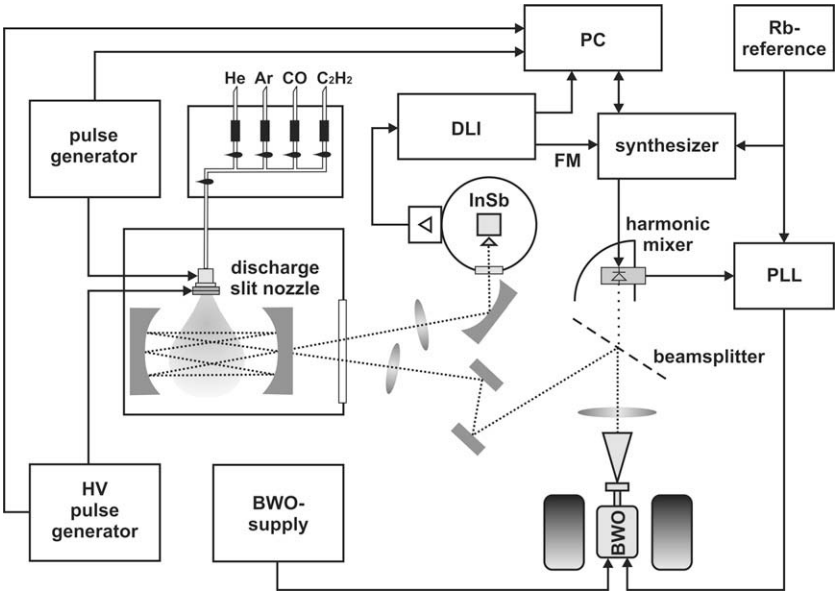

Fig. 2. Experimental setup of the Cologne Supersonic Jet Spectrometer for Terahertz Applications (SuJeSTA). Backward Wave Oscillators (BWOs) are used as radiation sources. The signal is detected on a liquid helium cooled InSb hot electron bolometer. A pulsed discharge slit nozzle produces C_3H radicals in a supersonic expansion of a C_2H_2/CO gas mixture diluted in He or Ar at 1–6 bar backing pressure. The probing microwave beam intersects the molecular jet in a multi-pass optics to enhance the absorption path length.

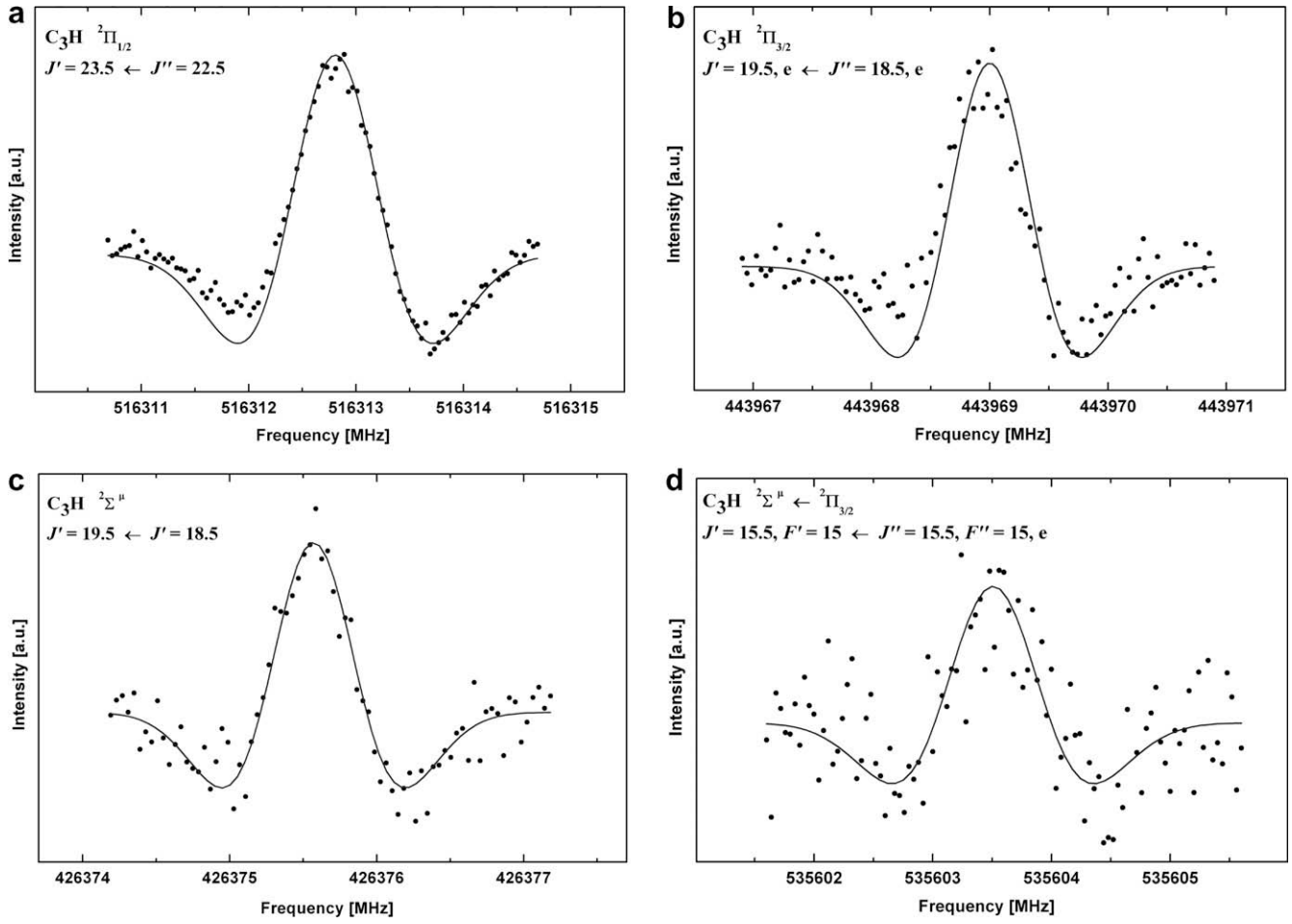

Fig. 3. C_3H spectral lines recorded in second derivative: pure rotational transition in the $^2\Pi_{1/2}$ state (a), in the $^2\Pi_{3/2}$ state (b), in the $^2\Sigma^{\mu}$ state (c), and ro-vibrational transition in the $\nu_4(^2\Sigma - {}^2\Pi_{3/2})$ band (d). Solid lines represent a fitted Gaussian line profiles in second derivative.

Table 1
Observed rotational transitions[a] within the $\Pi_{1/2}$ stack.

N	J	$p^b \leftarrow N$	J	p^b	Obs.[c]	$O-C$[d]	σ[e]
17	17.5	$e-\leftarrow 16$	16.5	$e+$	383435.0364	−0.0125	0.02
17	17.5	$f+\leftarrow 16$	16.5	$f-$	383942.3790	−0.0144	0.02
18	18.5	$e+\leftarrow 17$	17.5	$e-$	405547.3949	−0.0347	0.02
18	18.5	$f-\leftarrow 17$	17.5	$f+$	406095.4885	0.0055	0.02
19	19.5	$e-\leftarrow 18$	18.5	$e+$	427675.3334	0.0248	0.03
19	19.5	$f+\leftarrow 18$	18.5	$f-$	428263.6551	−0.0298	0.02
20	20.5	$e+\leftarrow 19$	19.5	$e-$	449817.1644	−0.0131	0.03
20	20.5	$f-\leftarrow 19$	19.5	$f+$	450445.4492	−0.0137	0.10
21	21.5	$e-\leftarrow 20$	20.5	$e+$	471971.5921	−0.0086	0.02
21	21.5	$f+\leftarrow 20$	20.5	$f-$	472639.3762	0.0078	0.03
22	22.5	$e+\leftarrow 21$	21.5	$e-$	494137.2040	−0.0205	0.03
22	22.5	$f-\leftarrow 21$	21.5	$f+$	494844.0555	0.0107	0.03
23	23.5	$e-\leftarrow 22$	22.5	$e+$	516312.7990	0.0178	0.02
24	24.5	$f-\leftarrow 23$	23.5	$f+$	539280.7450	0.0025	0.02

[a] The F quantum numbers have been omitted for transitions for which no hyperfine splitting was resolved.
[b] Parity of the levels are indicated by ±, with e/f labels.
[c] Observed frequencies in MHz.
[d] Observed − Calculated values in MHz.
[e] Estimated experimental uncertainties in MHz.

Table 2
Observed rotational transitions[a] within the $\Pi_{3/2}$ stack.

N	J	F	$p^b \leftarrow N$	J	F	p^b	Obs.[c]	$O-C$[d]	σ[e]
17	16.5		$f-\leftarrow 16$	15.5		$f+$	376303.9280	−0.0646	0.03
17	16.5		$e+\leftarrow 16$	15.5		$e-$	376705.8923	−0.0267	0.02
18	17.5		$f+\leftarrow 17$	16.5		$f-$	398879.3910	−0.0234	0.02
18	17.5		$e-\leftarrow 17$	16.5		$e+$	399288.8484	−0.0198	0.02
19	18.5		$f-\leftarrow 18$	17.5		$f+$	421433.9030	−0.0370	0.03
20	19.5		$f+\leftarrow 19$	18.5		$f-$	443968.9856	0.0436	0.03
20	19.5		$e-\leftarrow 19$	18.5		$e+$	444336.7031	0.0550	0.03
21	20.5		$f-\leftarrow 20$	19.5		$f+$	466485.7403	0.0243	0.03
21	20.5		$e+\leftarrow 20$	19.5		$e-$	466772.2477	−0.0441	0.04
22	21.5		$f+\leftarrow 21$	20.5		$f-$	488985.5099	0.0382	0.08
22	21.5		$e-\leftarrow 21$	20.5		$e+$	489095.5518	0.0667	0.08
23	22.5		$e+\leftarrow 22$	21.5		$e-$	511182.6138	0.0112	0.03
23	22.5		$f-\leftarrow 22$	21.5		$f+$	511469.3313	0.0040	0.05
24	23.5	24	$e-\leftarrow 23$	22.5	23	$e+$	532658.3010	0.1261	0.10
24	23.5	23	$e-\leftarrow 23$	22.5	22	$e+$	532658.8540	−0.2423	0.10
25	24.5	25	$e+\leftarrow 24$	23.5	24	$e-$	552384.8963	0.1679	0.20
25	24.5	24	$e+\leftarrow 24$	23.5	23	$e-$	552387.0137	−0.3070	0.20

[a,b,c,d,e] See footnotes of Table 1.

5. Analysis and results

In the present study, the energy levels of the ground vibronic state $^2\Pi$ and the lowest excited vibronic state $^2\Sigma^{\mu}$ have been calculated effectively neglecting all vibronic interactions with any other state. Hereafter, the two states are simply denoted as Π and Σ state, respectively. As discussed in the previous section, the Σ state is one component of the excited bending vibrational state, which is split by the Renner–Teller interaction. In the present analysis, however, we consider it effectively as an independent Σ vibronic state, more precisely, as a $^2\Sigma^+$ state, as mentioned in Section 2. Thus the effective Hamiltonian used here is the sum of the

Table 3
Observed rotational transitions[a] within the Σ stack.

N	J	F	$p^b \leftarrow N$	J	F	p^b	Obs.[c]	$O-C$[d]	σ[e]
17	16.5	17	$-\leftarrow 16$	15.5	16	+	381318.5540	−0.1347	0.10
17	16.5	16	$-\leftarrow 16$	15.5	15	+	381319.2560	−0.0890	0.10
17	17.5	18	$-\leftarrow 16$	16.5	17	+	381423.6383	−0.0818	0.05
17	17.5	17	$-\leftarrow 16$	16.5	16	+	381424.4022	0.0420	0.08
18	17.5		$+\leftarrow 17$	16.5		−	403735.4058	−0.0353	0.02
18	18.5		$+\leftarrow 17$	17.5		−	403887.7160	−0.0998	0.08
19	18.5		$-\leftarrow 18$	17.5		+	426148.7696	0.0046	0.03
19	19.5		$-\leftarrow 18$	18.5		+	426375.5900	−0.0459	0.10
20	19.5		$+\leftarrow 19$	18.5		−	448560.0278	0.1393	0.08
20	20.5		$+\leftarrow 19$	19.5		−	448907.7029	0.0144	0.03
21	21.5		$-\leftarrow 20$	20.5		+	471532.1665	−0.0207	0.03
23	23.5	23	$-\leftarrow 22$	22.5	22	+	517808.0271	0.1678	0.20
23	23.5	24	$-\leftarrow 22$	22.5	23	+	517808.7324	−0.0771	0.20

[a,c,d,e]See footnotes of Table 1.
[b] The *e*/*f* symbols are not indicated because the $^2\Sigma^\mu$ state is well represented as the case (*b*) $^2\Sigma^+$ state.

rotation–vibration, spin–orbit coupling, Λ-type doubling, spin–rotation coupling, hyperfine contribution, and the vibronic interaction between the Π and Σ state:

$$\widehat{\mathscr{H}} = \widehat{\mathscr{H}}_{\text{rovib}} + \widehat{\mathscr{H}}_{\text{SO}} + \widehat{\mathscr{H}}_{\Lambda} + \widehat{\mathscr{H}}_{\text{SR}} + \widehat{\mathscr{H}}_{\text{hf}} + \widehat{\mathscr{H}}_{\text{int}}. \tag{2}$$

The ro-vibrational part is expressed for the two vibronic states as

$$\widehat{\mathscr{H}}_{\text{rovib}} = E + B(\widehat{\boldsymbol{N}}^2 - \widehat{N}_z^2) - D(\widehat{\boldsymbol{N}}^2 - \widehat{N}_z^2)^2 + H(\widehat{\boldsymbol{N}}^2 - \widehat{N}_z^2)^3, \tag{3}$$

where E represents the energy difference between the excited $^2\Sigma^+$ state and the $^2\Pi$ level for $A_{\text{SO}} = 0$. The centrifugal distortion correction terms required to fit the present data are included as the power series expansion on $\widehat{\boldsymbol{N}}^2$ here and for the fine and hyperfine terms as well. In the present analysis, we use Pickett's SPFIT program [17] where the matrix elements are calculated on Hund's case (*b*) basis. Thus, $\widehat{N}_z$, the axis component of the sum of the electronic orbital angular momentum and the vibrational angular momentum, is diagonal on this basis set, and simply expressed by K which is $\Lambda + \ell$, with $K = \pm 1$ for the Π and $K = 0$ for the Σ state.

The spin–orbit interaction and the Λ-type doubling interaction contribute only to the matrix elements for the Π state. They are

$$\widehat{\mathscr{H}}_{\text{SO}} = A_{\text{SO}}\widehat{\boldsymbol{L}}\cdot\widehat{\boldsymbol{S}}, \tag{4}$$

$$\widehat{\mathscr{H}}_{\Lambda} = -\frac{1}{2}p\left(\widehat{N}_+\widehat{S}_+ + \widehat{N}_-\widehat{S}_-\right) - \frac{1}{4}p_D\left[\widehat{N}_+\widehat{S}_+ + \widehat{N}_-\widehat{S}_-, \widehat{\boldsymbol{N}}^2\right]_+ + \frac{1}{2}q\left(\widehat{N}_+^2 + \widehat{N}_-^2\right) + \frac{1}{4}q_D\left[\widehat{N}_+^2 + \widehat{N}_-^2, \widehat{\boldsymbol{N}}^2\right]_+, \tag{5}$$

where the matrix elements should be only considered between the $\Lambda = +1$ and -1 state.

The spin–rotation coupling term, which contributes effectively to both Π and Σ state in the present case, is

$$\widehat{\mathscr{H}}_{\text{SR}} = \gamma\widehat{\boldsymbol{N}}\cdot\widehat{\boldsymbol{S}} + \frac{1}{2}\gamma_D\left[\widehat{\boldsymbol{N}}\cdot\widehat{\boldsymbol{S}}, \widehat{\boldsymbol{N}}^2\right]_+. \tag{6}$$

The nuclear hyperfine splitting caused by the proton is evaluated by

$$\widehat{\mathscr{H}}_{\text{hf}} = a\widehat{\boldsymbol{I}}\cdot\widehat{\boldsymbol{L}} + b_F\widehat{\boldsymbol{I}}\cdot\widehat{\boldsymbol{S}} + \frac{c}{3}(3I_zS_z - \widehat{\boldsymbol{I}}\cdot\widehat{\boldsymbol{S}}) - \frac{d}{2}(\widehat{S}_+\widehat{I}_+ + \widehat{S}_-\widehat{I}_-), \tag{7}$$

where the off-diagonal spin–spin interaction term, i.e. the term with d, should be only taken into account between the $\Lambda = +1$ and -1 state.

An interaction term is introduced between the Π and Σ vibronic state as

$$\widehat{\mathscr{H}}_{\text{int}} = -\beta\left(\widehat{N}_+\widehat{L}_- + \widehat{N}_-\widehat{L}_+\right) - \beta_D\left[\widehat{N}_+\widehat{L}_- + \widehat{N}_-\widehat{L}_+, \widehat{\boldsymbol{N}}^2\right]_+, \tag{8}$$

which is the L-uncoupling interaction. In the present case, the $L_\pm$ should be interpreted as the ladder operator for the vibrational angular momentum. Eq. (8) is equivalent to that given by Yamamoto et al. [7] but represented by $\boldsymbol{N}$ instead of $\boldsymbol{J}$. Since the centrifugal distortion correction on this parameter has been found significant, the term with β_D is added in Eq. (8).

The symbols for the fine and hyperfine constants are expressed in the equations above by following the IUPAC recommendation [18,19]. It should be noted that the spectroscopic parameters obtained directly from the SPFIT program are not always identical to those given in Eq. (4)–(8). We have cross-checked the correspondence of the parameters in the Hamiltonian and those in the program by an independent program system, PGOPHER, which is open to the public [20].

Least-squares fits have been applied to the set of measured lines including the data from Kaifu et al. [21], Gottlieb et al. [22] and Yamamoto et al. [7]. In the weighted least-squares fit, the uncertainties of the lines of Refs. [22,7] were set to 50 kHz.

The rotational constant B, the centrifugal distortion term D, the electronic spin–rotation interaction constant γ, the Fermi-contact interaction parameter b_F, and the dipole–dipole coupling constant c have been determined for both the $^2\Pi$ and $^2\Sigma^\mu$ states. The Λ-type doubling constants p and q, their centrifugal correction constants p_D and q_D, the hyperfine constant a and d, and the spin–orbit interaction constant A_{SO} have been determined for the $^2\Pi$ state. The centrifugal distortion correction on the spin–rotation interaction constant, γ_D, was significant only in the $^2\Sigma^\mu$ state. The sextic centrifugal distortion constant H was determined for the ground $^2\Pi$ state.

As mentioned in Section 4, the hyperfine splitting was not resolved for most of the lines. For those lines, the observed line positions are compared with the line centers calculated from the hyperfine components by the intensity-weighted-average.

The parameter values determined by the present study are listed in Table 5. The vibronic interaction constant β and the energy term of the $^2\Sigma^\mu$ state have been determined with much higher precision than those reported by Yamamoto et al. [7]. In addition, the centrifugal distortion correction β_D for the interaction constant has been determined with significance.

Table 4
Observed rotational transitions[a] between the Π and Σ stack.

Term	N	J	F	$p^b \leftarrow$ term	N	J	F	p^b	Obs.[c]	$O-C$[d]	σ[e]
Σ	16	15.5	16	$+\leftarrow \Pi_{3/2}$	16	15.5	16	$e-$	535599.9212	−0.0252	0.08
Σ	16	15.5	15	$+\leftarrow \Pi_{3/2}$	16	15.5	15	$e-$	535603.5071	−0.0319	0.07
Σ	17	16.5	17	$-\leftarrow \Pi_{3/2}$	17	16.5	17	$e+$	540212.6576	−0.0193	0.09
Σ	17	16.5	16	$-\leftarrow \Pi_{3/2}$	17	16.5	16	$e+$	540217.0723	0.0655	0.08
Σ	18	17.5	18	$+\leftarrow \Pi_{3/2}$	18	17.5	18	$e-$	544659.4669	0.0158	0.10
Σ	25	25.5	26	$-\leftarrow \Pi_{3/2}$	25	24.5	25	$e+$	569212.4912	−0.0580	0.06
Σ	25	25.5	25	$-\leftarrow \Pi_{3/2}$	25	24.5	24	$e+$	569216.5411	0.0752	0.06
$\Pi_{3/2}$	26	25.5	26	$e-\leftarrow\Sigma$	24	24.5	25	+	571024.5676	−0.0016	0.03

[a,c,d,e]See footnotes of Table 1.
[b] The *e*/*f* symbols are not indicated for the Σ state because this state is well represented as the case (*b*) $^2\Sigma^+$ state.

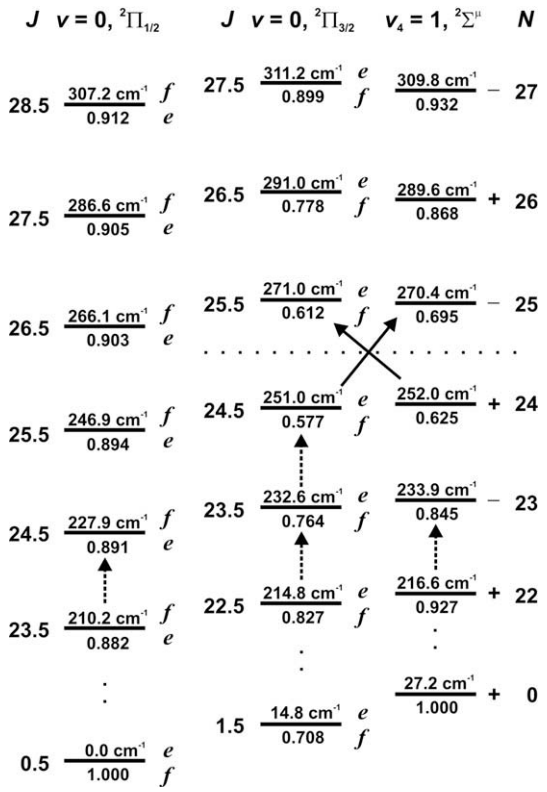

Fig. 4. Energy levels of the $^2\Pi$ and vibrational excited $^2\Sigma$ states. The ro-vibrational energy in wavenumbers is given above the energy levels. Pure rotational transitions observed within a state are indicated as dashed arrows, ro-vibrational transitions are indicated as solid arrows. The dotted line marks the position of the $^2\Sigma^\mu/^2\Pi_{3/2}$ energy level crossing at 261.5 cm^{-1} where transitions between the Π and Σ state were found to be enhanced by vibronic interaction.

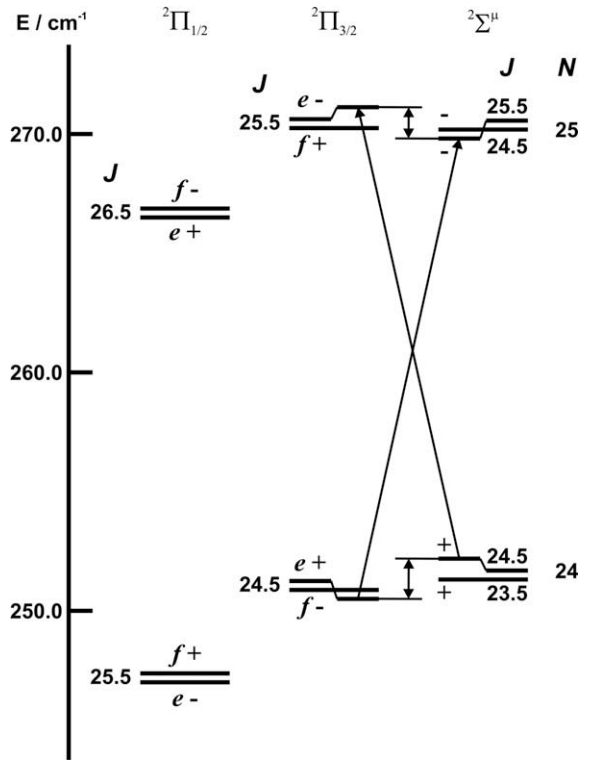

Fig. 5. Energy levels of $^2\Pi$ and vibrational excited $^2\Sigma$ states near the resonance. The energy order of the $J = 24.5$ ($^2\Pi_{3/2}$) Λ-doublet and the $N = 25$ ($^2\Sigma^\mu$) spin doublet is inverted due to vibronic interactions. ± parity labels are used according to a Σ^μ state with Σ^+ symmetry (see text).

The dimensionless standard deviation of the final fit was ~1.0. The accuracy of molecular parameters revised in the present study allows to predict transition frequencies beyond 1 THz within Doppler limited line widths. All related data will be made available in the Fitting Spectra section of the Cologne Database for Molecular Spectroscopy (CDMS) [23,24] while the predictions will be provided in the catalog section [25].

6. Discussion

Ro-vibrational transitions between the v_4 excited $^2\Sigma^\mu$ state and the ground $^2\Pi_{3/2}$ state have been observed for the first time. In addition, the present work extends the previous investigations of pure rotational transitions within the $\Pi_{1/2}$ and $\Pi_{3/2}$ bands, and in the vibrational excited $^2\Sigma^\mu$ state up to 539 GHz. The molecular constants have been revised as given in Table 5. The present study confirms the parameter values reported by Yamamoto et al. [7] which are also listed in the table.

The observation of ro-vibrational transitions $v_4 = 1 \leftarrow 0(^2\Sigma^\mu \leftarrow {}^2\Pi_{3/2})$ yielded a very accurate term value for the $^2\Sigma^\mu$ state, compared to the uncertainty of more than 1 GHz reported previously [7]. Additionally, the accuracy of the vibronic interaction constant β has been improved.

It is worthwhile mentioning that the sign of β cannot be determined from the line positions because the perturbation is purely off-diagonal. Its sign can be determined from observed relative intensities of suitable resonance enhanced transitions, if the signs and the magnitudes of the permanent dipole moment and the dipole moment derivative of the bending mode are available. Otherwise, its sign can be determined *relative* to the chosen signs of the

Table 5
Spectroscopic parameters of C_3H determined in the present study.[a,b]

Parameter	Present work	Yamamoto et al.	Unit
Ground state ($^2\Pi$))			
B	11189.1033 (84)	11189.052 (48)	MHz
D	5.2340 (127)	5.1365 (50)	kHz
H	0.02276 (196)	–	Hz
A_{SO}	432.7898 (84)	432.834 (31)	GHz
γ	−48.075 (117)	−48.57 (126)	MHz
p	−7.0681 (25)	−7.0842 (97)	MHz
p_D	0.504 (138)	1.41 (74)	kHz
q	−12.9922 (104)	−13.057 (67)	MHz
q_D	−0.1432 (224)	–	kHz
a	12.318 (155)	12.33 (23)	MHz
b_F	−13.683 (98)	−13.38 (70)[c]	MHz
c	28.07 (32)	27.49 (97)	MHz
d	16.2578 (28)	16.241 (27)	MHz
Excited state ($^2\Sigma^\mu$)			
E	609.9742 (41)	610.197 (1230)	GHz
B	11212.6703 (162)	11212.764 (96)	MHz
D	4.867 (23)	5.0066 (85)	kHz
γ	−35.525 (25)	−35.454 (96)	MHz
γ_D	0.549 (155)	1.45 (79)	kHz
b_F	1.450 (137)	1.4 (28)[c]	MHz
c	27.17 (48)	28.5 (26)	MHz
Vibronic interaction[d]			
β	1234.2 (19)	1224 (123)	MHz
β_D	−19.2 (29)	–	kHz

[a] The symmetry of $^2\Sigma^\mu$ is assumed to be $^2\Sigma^+$, which is consistent with the choice of Yamamoto et al. [7]. If it is $^2\Sigma^-$, signs of p, p_D, q, q_D, and d for the Π state should be simultaneously inverted.

[b] Numbers in the parentheses are one standard deviation.

[c] Derived by using $b_F = b + c/3$.

[d] Since the sign of the interaction constant can not be determined, β is assumed to be positive, see also text; the signs for β and β_D can be inverted simultaneously.

corresponding dipole moments (or their components) as done, e.g., in Refs. [26–28]. Although the intensities have not been measured accurately in the present study, the transition $(\Gamma,N,J,F) = (\Pi_{3/2},26,25.5,26) \leftarrow (\Sigma,24,24.5,25)$ is observed to be significantly stronger than $(\Gamma,N,J,F) = (\Sigma,25,25.5,26) \leftarrow (\Pi_{3/2},25,24.5,25)$. A simple model calculation of two level-interaction scheme suggests qualitatively β to be positive, on the basis of the observed intensity difference mentioned above and the fact that the dipole moment derivative of a bending mode is always positive. Thus, we derive tentatively a positive sign for β, in contrast to the assumed sign in Yamamoto et al. [7].

The symmetry of $^2\Sigma^{\mu}$ is assumed to be $^2\Sigma^+$ in the present study as mentioned in Section 2. The *e*/*f* labels of the $^2\Pi_{3/2}$ states were then determined by the selection rule of the vibronic interaction. This allows us to determine the signs of the parameter p, p_D, q, q_D, and d for the Π state as listed in Table 5. If the $^2\Sigma^{\mu}$ state is $^2\Sigma^-$, the signs of those parameters should be inverted simultaneously.

The spin–orbit coupling constant A_{SO} is now determined with improved precision. The value of the spin–orbit coupling constant has been predicted by quantum-chemical calculations to be approximately twice as large as the experimental value of A_{SO} in Ref. [13].

The derived hyperfine structure parameters are in good agreement with those of Yamamoto et al. but show large deviations from the theoretical values of Perić et al. [29] and Mladenović et al. [30].

All parameters obtained in this work have smaller uncertainties than those of earlier work and are very reliable for frequency predictions up to 1 THz. In particular the uncertainties of transitions near the $v_4 = 1/v = 0$ crossing decreased from 1 GHz to a few 10 kHz compared to predictions based on the parameter set of Ref. [7]. Thus present result encourages further searching for ro-vibrational bending transitions of C_3H in the interstellar and circumstellar medium.

SuJeSTA has been designed to be operated with different molecular sources for producing molecular radicals and ions. A laser ablation source will allow measurements on many transient molecules, such as pure carbon and silicon–carbon clusters [31–35]. Symmetric molecules and ions, which have no permanent dipole moments, and thus no pure rotational spectra, will be studied by their ro-vibrational transitions. Many carbon chain molecules, such as linear C_3 [36] or C_7 [37], have energetically low lying bending modes, which transitions can be used for their detection in space [38]. New telescopes, like instruments onboard the Herschel satellite or the Stratospheric Observatory for Infrared Astronomy, SOFIA, will be used to search for such new species, once their spectra are known from laboratory measurements.

Acknowledgments

The present investigation was supported by the Laboratoire Européen Associé (LEA) *HiRes*, administered by the Deutsche Forschungsgemeinschaft (DFG) via Grant GI 319/1-1. Additional funding has been provided by DFG via Grant SFB 494. The authors thank Dr. C. Western for many instructive and helpful suggestions concerning his PGOPHER program system. M.C. and C.D. are grateful to LEA and the Humboldt-Foundation, respectively, for their financial support. H.S.P.M. thanks the Bundesministerium für Bildung und Forschung (BMBF) for funding which was administered through Deutsches Zentrum für Luft- und Raumfahrt (DLR). K.M.T.Y. is grateful to DFG for supporting his stay in Cologne.

Appendix A. Supplementary data

Supplementary data for this article are available on ScienceDirect (www.sciencedirect.com) and as part of the Ohio State University Molecular Spectroscopy Archives (http://library.osu.edu/sites/msa/jmsa_hp.htm). Supplementary data associated with this article can be found, in the online version, at doi:10.1016/j.jms.2008.10.006.

References

[1] J. Cernicharo, J.R. Goicoechea, E. Caux, Astrophys. J. 534 (2000) L199.
[2] T.F. Giesen, A.O. Van Orden, J.D. Cruzan, R.A. Provencal, R.J. Saykally, R. Gendriesch, F. Lewen, G. Winnewisser, Astrophys. J. 551 (2001) L181.
[3] L. Johansson, C. Andersson, J. Elder, P. Friberg, A. Hjalmarson, B. Hoglund, W. Irvine, H. Olofsson, G. Rydbeck, Astron. Astrophys. 130 (1984) 227.
[4] P. Thaddeus, C.A. Gottlieb, Astrophys. J. 294 (1985) L49.
[5] C.A. Gottlieb, J.M. Vrtilek, E.W. Gottlieb, P. Thaddeus, A. Hjalmarson, Astrophys. J. 294 (1985) L55.
[6] S. Yamamoto, S. Saito, A. Murakami, Astrophys. J. 322 (1987) L55.
[7] S. Yamamoto, S. Saito, H. Suzuki, S. Deguchi, N. Kaifu, S. Ishikawa, M. Ohishi, Astrophys. J. 348 (1990) 363.
[8] M. Kanada, S. Yamamoto, S. Saito, Y. Osamura, J. Chem. Phys. 104 (1996) 2192.
[9] M. McCarthy, P. Thaddeus, J. Chem. Phys. 122 (2005) 174308.
[10] H. Ding, T. Pino, F. Güthe, J.P. Maier, J. Chem. Phys. 115 (2001) 6913.
[11] S.M. Sheehan, B.F. Parsons, J. Zhou, E. Garand, T.A. Yen, D.T. Moore, D.M. Neumark, J. Chem. Phys. 128 (2008) 034301.
[12] Q. Jiang, C.M.L. Rittby, W.R.M. Graham, J. Chem. Phys. 99 (1993) 3194.
[13] M. Perić, M. Mladenović, K. Tomić, C.M. Marian, J. Chem. Phys. 118 (2003) 4444.
[14] C. Jungen, A. Merer, in: K. Narahari Rao (Ed.), Molecular Spectroscopy: Modern Research, vol. II, Academic Press, 1976.
[15] J.T. Hougen, J. Chem. Phys. 36 (1962) 519.
[16] T. Motylewski, H. Linnartz, Rev. Sci. Instrum. 70 (1999) 1305.
[17] H.M. Pickett, J. Mol. Spectrosc. 148 (1991) 371.
[18] E. Hirota, J. Brown, J. Hougen, T. Shida, N. Hirota, Pure Appl. Chem. 66 (1994) 571.
[19] E. Hirota, J.M. Brown, J.T. Hougen, T. Shida, N. Hirota, J. Mol. Spectrosc. 168 (1994) 628.
[20] PGOPHER, C.M. Western, 2008. Available from: <http://pgopher.chm.bris.ac.uk/>.
[21] N. Kaifu, M. Ohishi, K. Kawaguchi, S. Saito, S. Yamamoto, T. Miyaji, K. Miyazawa, S. Ishikawa, C. Noumaru, S. Harasawa, et al., Publ. Astron. Soc. Jpn. 56 (2004) 69.
[22] C.A. Gottlieb, E.W. Gottlieb, P. Thaddeus, J.M. Vrtilek, Astrophys. J. 303 (1986) 446.
[23] H.S.P. Müller, S. Thorwirth, D.A. Roth, G. Winnewisser, Astron. Astrophys. 370 (2001) L49.
[24] H.S.P. Müller, F. Schlöder, J. Stutzki, G. Winnewisser, J. Mol. Struct. 742 (2005) 215.
[25] CDMS, 2008. Available from: <http://www.cdms.de>.
[26] D. Christen, H.S.P. Müller, Phys. Chem. Chem. Phys. 5 (2003) 3600.
[27] H.S.P. Müller, D. Christen, J. Mol. Spectrosc. 228 (2004) 298.
[28] C.P. Endres, H.S.P. Müller, S. Brünken, D.G. Paveliev, T.F. Giesen, S. Schlemmer, F. Lewen, J. Mol. Struct. 795 (2006) 242.
[29] M. Perić, M. Mladenović, B. Engels, J. Chem. Phys. 121 (2004) 2636.
[30] M. Mladenović, M. Perić, B. Engels, J. Chem. Phys. 121 (2004) 12361.
[31] P. Neubauer-Guenther, T.F. Giesen, U. Berndt, G. Fuchs, G. Winnewisser, Spectrochim. Acta A 59 (2002) 431.
[32] T.F. Giesen, U. Berndt, K.M.T. Yamada, G. Fuchs, R. Schieder, G. Winnewisser, R.A. Provencal, F.N. Keutsch, A. Van Orden, R.J. Saykally, Chem. Phys. Chem. 2 (2001) 242.
[33] T.F. Giesen, A.V. Orden, H.J. Hwang, R.S. Fellers, R.A. Provencal, R.J. Saykally, Science 265 (1994) 756.
[34] A.V. Orden, T.F. Giesen, R.A. Provencal, H.J. Hwang, R.J. Saykally, J. Chem. Phys. 101 (1994) 10237.
[35] A.V. Orden, R.A. Provencal, T.F. Giesen, R.J. Saykally, Chem. Phys. Lett. 237 (1995) 77.
[36] R. Gendriesch, K. Pehl, T. Giesen, G. Winnewisser, F. Lewen, Z. Naturforsch. 58 (2003) 129.
[37] P. Neubauer-Guenther, T.F. Giesen, S. Schlemmer, K.M.T. Yamada, J. Chem. Phys. 127 (2007) 014313.
[38] T.F. Giesen, S. Brünken, M. Caris, P. Neubauer-Guenther, U. Fuchs, G.W. Fuchs, F. Lewen, in: G.A. Blake, E. Herbst, D.C. Lis (Eds.), Astrochemistry: Recent Successes and Current Challenges, Proceedings of the International Astronomical Union, Cambridge University Press, 2005, pp. 87–96.